


RESEARCH

Open Access



Theoretical evaluation of stack-based thermoacoustic refrigerators

B. G. Prashantha^{1*} , G. S. V. L. Narasimham², S. Seetharamu³ and Vinayak B. Hemadri⁴

Abstract

Standing wave thermoacoustic refrigerator uses stack, is the heart of the thermoacoustic cooling system. The porous stack in the resonator tube develops temperature difference across the stack for heat pumping upon loudspeaker sound interaction of oscillating gas. In this paper, the optimization of stack-heat exchangers system and resonator is discussed using linear thermoacoustic theory for better COP and cooling power of refrigerator. The loudspeaker is assumed to provide the required acoustic power with the back volume gas spring system. Helium and air are chosen because of their better thermophysical properties and cost, compared to other competent gases. The 200 mm diameter stack is optimized for the temperature difference of 28 K. The theoretical results of the optimized refrigerator models are compared with the DeltaEC simulation results for deriving conclusions. DeltaEC predicts the cooling power and COP of 349 W at 0.998 for helium, and 139 W at 1.133 for air, respectively.

Keywords: Spiral stack-heat exchangers, Stack length and center combination, Porosity, TDH resonator

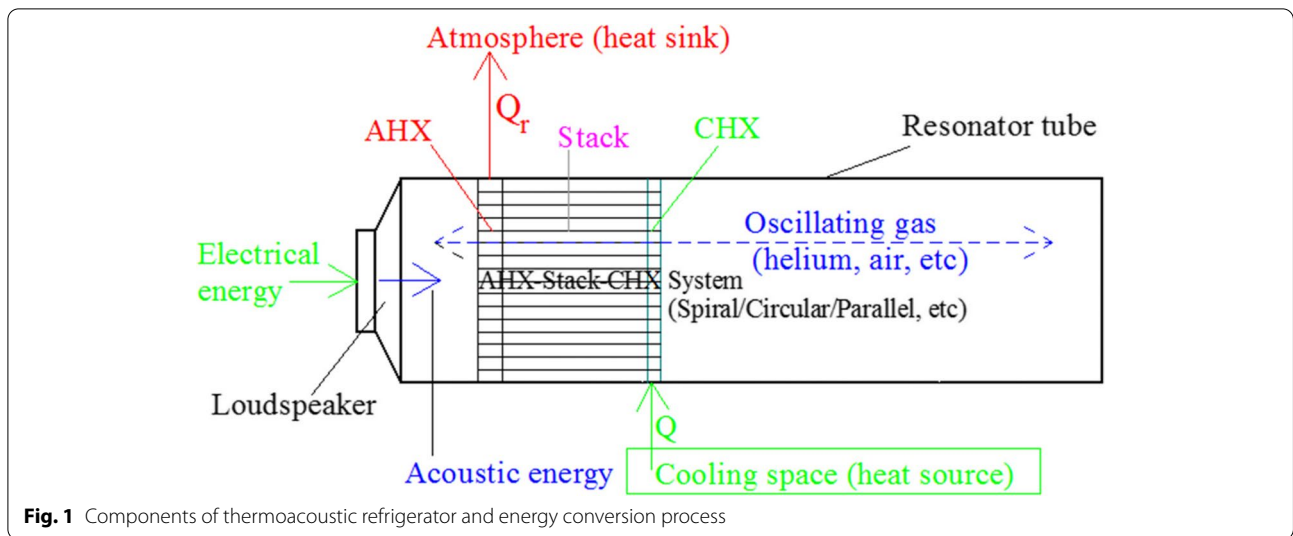
1 Introduction

In the recent years, the research on thermoacoustic cooling has given impetus on optimizing the devices theoretically as well as building practically. Thermoacoustic cooling is considered as an alternative technology to replace the present dominant vapor compression units in the commercial world. It is a promising cooling technology compared to the other unconventional technologies because of its simplicity of construction, benign working substances and absence of moving parts, can be built with the indigenous materials, etc. Thermoacoustic effect is the interconversion of sound and heat energies happens in thermoacoustic devices. Thermoacoustic devices are of either thermoacoustic engines or refrigerators. Thermoacoustic engine convert heat input into acoustic work output, whereas the thermoacoustic refrigerator convert acoustic work input into refrigeration effect. Thermoacoustic refrigerator pumps heat from cold space to surrounding environment

to produce refrigeration effect upon acoustic energy input. Thermoacoustic refrigerator is either powered by thermoacoustic engine called thermo-acoustically driven thermoacoustic refrigerator, or by loudspeaker called acoustically driven thermoacoustic refrigerator. The loudspeaker-driven thermoacoustic refrigerators (LDTAR) are quite promising and popular compared to the engine-driven (thermo-acoustically driven) thermoacoustic refrigerators (EDTAR) because of simplicity in construction and operations [1]. The schematic showing the components, oscillating gas, and energy conversion process in thermoacoustic refrigerator is shown in Fig. 1. Electro-acoustic energy conversion happens in the moving coil loudspeaker and supplies sound energy to the resonator contains a stack-heat exchangers system and pressurized gas (helium, air, or any other inert gas) at 10 bar [2]. The acoustic standing wave generated by loudspeaker causes gas to oscillate front and back through the small pores of the stack-heat exchangers system. The ambient and cold heat exchangers are placed on either side of the stack as shown in Fig. 1. The position of the stack-heat exchangers system in a resonator depends on the maximum compression and rarefaction regions.

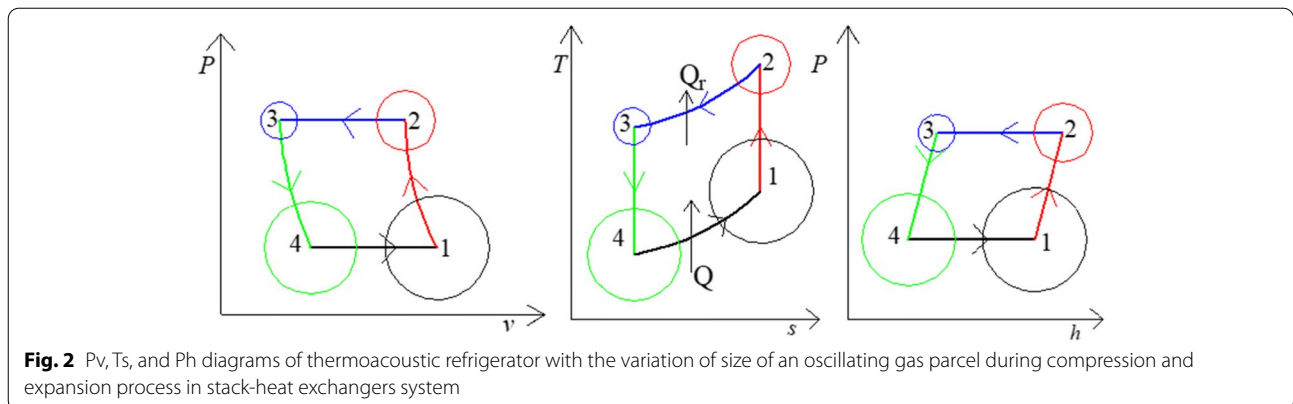
*Correspondence: bgpsandur@gmail.com

¹ Department of Mechanical Engineering, JSS Academy of Technical Education, Dr. Vishnuvardhana Road, Bengaluru 560 060, India
Full list of author information is available at the end of the article



The stack-heat exchangers system is placed such that the ambient heat exchanger (AHX) is at the maximum compression region and the cold heat exchanger (CHX) is at the maximum rarefaction region [3, 4]. The successive gas oscillation pumps heat from CHX to AHX through stack produces temperature gradient across the stack (Fig. 1). The heat pumping mechanism in the stack-heat exchangers system is depicted with Pv , Ts , and Ph diagrams (Fig. 2), which is similar to Brayton cycle. It has two isentropic processes and two isobaric processes. The process 1–2 compresses gas isentropically and the compressed gas reject heat at constant pressure (process 2–3) to the AHX plates maintained at ambient temperature by water cooling system. The above two processes happen in the forward movement of the gas. In the reverse movement of the gas, it expands isentropically (process 3–4), and the cold gas absorbs heat from the CHX plates connected to cooling space at constant pressure (process 4–1). The cycle repeats and the variation of the size of the oscillating gas at the state points 1–2–3–4 are also shown (Fig. 2).

In this paper, an attempt is made to explain the method of optimizing stack-heat exchangers system in terms of the normalized stack length and center positions with helium and air considering the performance of the refrigerator compared to the published literature [5–8]. The spiral geometry is chosen for the stack-heat exchangers system because of its simplicity and ease of construction during fabrication compared to other geometries (parallel plate, circular, pin array, etc.) [4, 5]. Also, the performance of the spiral geometry expressed in terms of half stack spacing distance y and thermal penetration depth δ_k is on par with parallel plate geometry at $y=2\delta_k$ for helium and $y=\delta_k$ for air [6]. The cooling capacity of the refrigerator increases with increase in size of the refrigerator and at the same time performance of the stack and refrigerator decreases, and vice versa [7]. The stack center position X is the distance between the loudspeaker position and the mid-point of the stack length l_3 . The performance of the stack increases with decrease in stack center position



and length. Because the decrease in stack center position and length decreases the acoustic wave disturbance of the oscillating gas in the stack region of the cooler. Hence, the presence of the small length of the stack will offer minimum resistance for the oscillating gas, leading to improvement in the performance of the stack as found in the published literature [4, 8]. In the published literature [3, 4, 7, 8], the stack-heat exchangers system is optimized by choosing the stack length and center position merely based on the highest performance of the stack. This makes the device compact and improves power density with poor cooling capacity of the refrigerator. The highest performance of the stack is chosen at the lowest possible stack length and center position such that which ensures the space for accommodating AHX and instrumentation between the hot end of the stack and loudspeaker [9, 10].

The scope of the present work is limited to the design, analysis, optimization, and theoretical evaluation of the standing wave LDTAR systems [11]. The objectives of the current research work are to optimize the spiral stack-heat exchangers system with helium and air, not merely at highest stack performance, but also at better cooling power and power density of the refrigerator compared to the published literature [8]. This is achieved by wisely choosing the next higher value for the normalized stack length and center position such that small drop in stack performance returns with drastic improvement in cooling capacity. Because the small increase in stack length and center position dramatically relieves acoustic resistance in the stack-heat exchangers system. The small drop in stack performance is because of viscous losses of the oscillating gas in the stack-heat exchangers system. The optimization

techniques for the stack-heat exchangers system are discussed in Sect. 2. The small drop in power density of the refrigerator model at the higher chosen value of the normalized stack length and center position is compensated while optimizing the resonator system discussed in Sect. 3. The loudspeaker optimization to improve electro-acoustic efficiency using back volume gas spring system discussed in Sect. 4. The theoretically optimized standing wave refrigerator models with helium and air as oscillating gases are tested in DeltaEC software [12] for validation discussed in Sect. 5 and the conclusions are drawn in Sect. 6.

2 Design and optimization of stack-heat exchangers system

In this section the design and optimization of the stack, cold and ambient heat exchangers having spiral geometry with 85% porosity to minimize acoustic field disturbances to improve cooler performance compared to 75% porosity is discussed [7, 8]. The geometry and cross section of the stack and heat exchangers is same except the length. Hence the design and optimization techniques are same for stack, CHX and AHX except the material selection. The stack materials should not conduct heat in the direction opposite to heat pumping process (ambient end to cold end) (Fig. 1) which decreases stack performance. Hence, the locally available Mylar sheets have reasonable cost and low thermal conductivity ($0.15 \text{ Wm}^{-1} \text{ K}^{-1}$) for the stack, and copper sheets for the cold and ambient heat exchangers ($401 \text{ Wm}^{-1} \text{ K}^{-1}$), is chosen for better performance [5, 13]. The cross section of the spirally wound Mylar stack and copper heat exchangers is shown in Fig. 3. The thin Mylar sheet is wound over

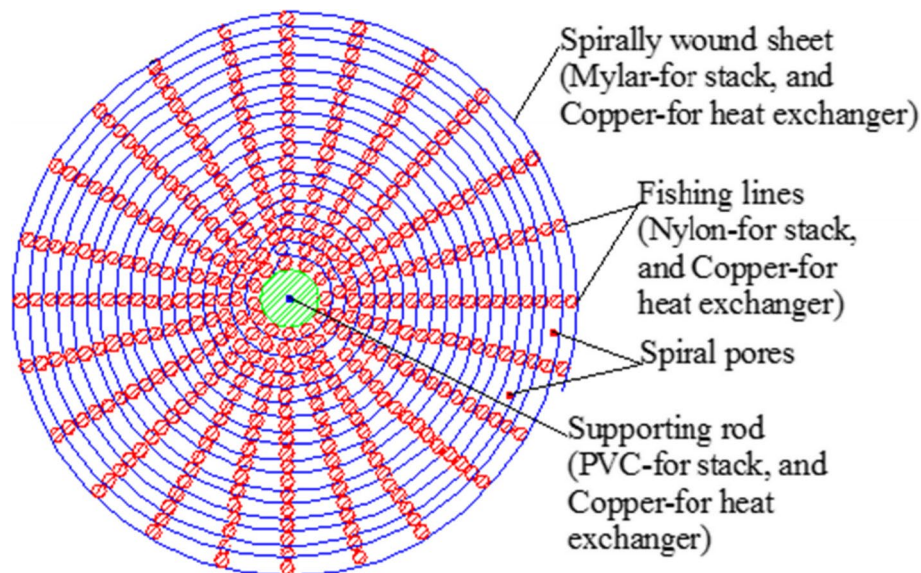


Fig. 3 Cross-section showing the spiral geometry for stack and heat exchangers system

Table 1 Design requirements, operating parameters, and thermophysical properties of gas

Cooler design parameters	Thermophysical properties of gas	
	Helium	Air
Design requirements: $\theta = 28$ K, $d_1 = 200$ mm, Operating parameters: $D = 3\%$, $P = 10$ bar, $T_{mg} = 288$ K, $T_{ax} = 301$ K, $f = 400$ Hz (helium), $f = 200$ Hz (air), $\varepsilon = 0.85$	$u = 998.6$ ms ⁻¹ , $\rho = 1.6715$ kgm ⁻³ , $C_p = 5193.4$ Jkg ⁻¹ K ⁻¹ , $C_v = 3109.8$ Jkg ⁻¹ K ⁻¹ , $\mu = 1.9392E - 5$ kgm ⁻¹ s ⁻¹ , $\delta_v = 9.609E - 5$ m, $k_g = 14.804E - 2$ Wm ⁻¹ K ⁻¹ , $\delta_k = 11.65E - 5$ m $\gamma = 1.67$	$u = 340.2$ ms ⁻¹ , $\rho = 12.096$ kgm ⁻³ , $C_p = 1004.7$ Jkg ⁻¹ K ⁻¹ , $C_v = 717.6$ Jkg ⁻¹ K ⁻¹ , $\mu = 1.7887E - 5$ kgm ⁻¹ s ⁻¹ , $\delta_v = 4.851E - 5$ m, $k_g = 2.5302E - 2$ Wm ⁻¹ K ⁻¹ , $\delta_k = 5.756E - 5$ m $\gamma = 1.4$

the supporting 10 mm PVC rod (0.19 Wm⁻¹ K⁻¹) with a thin Nylon wire (0.24 Wm⁻¹ K⁻¹) as fishing lines to provide spacing for the oscillating gas. Similarly for heat exchangers the thin Copper sheet is wound over the supporting 10 mm Copper rod with a thin Copper wire as fishing lines.

The design requirements, operating parameters of the refrigerator and thermophysical properties of the oscillating helium and air is given in Table 1. The derived parameters used in the design process and their values obtained using the data given in Table 1 are given in Table 2. In standing wave thermoacoustic engine or cooler, the term which decides performance is the critical temperature difference between ambient and cold heat exchangers, θ_c . At critical temperature, the stack does not pump heat because of zero temperature difference θ between ambient and cold heat exchangers. Critical temperature difference between ambient and cold heat exchangers is measured per unit length of the stack which is given by

$$\theta_c = \frac{(\gamma - 1)\varepsilon c T_{mg}}{\tan(cX)} \quad (1)$$

The normalization of design parameters is employed to simplify the design process by reducing the number of parameters involved in optimizing the stack-heat exchangers system [14]. While optimizing stack-heat exchangers system, the basic seventeen design

parameters (Table 1) and the seven derived parameters (Table 2) are reduced to eleven as shown in Table 3. They are the drive ratio D (ratio of acoustic pressure amplitude to average pressure), normalized temperature gradient θ_n (ratio of temperature gradient to mean temperature of gas between heat exchangers) and normalized critical temperature gradient Γ (ratio of temperature gradient to critical temperature gradient between ambient and cold heat exchangers).

The ambient heat exchanger length l_2 , stack length l_3 , cold heat exchanger length l_4 , and stack center position X are normalized with the subscript n by multiplying with wave number of gas, c . The thermal and viscous penetration depths (δ_k and δ_v) are normalized with the subscript n by dividing with half-spiral stack-heat exchangers sheets spacing, y . Similarly, the cooling power (Q) and acoustic power (W) are normalized with the subscript n by dividing with the product of (PuA). In the design process, the thermal conductivity of stack materials is neglected, and for helium and air the product of T_{mg} is set equal to one. Using the normalized design parameters (Table 3), the normalized heat output (Q_{ns}) and acoustic work input (W_{ns}) equations obtained using Rott's thermoacoustic theory [13, 15] is given by

Table 3 Normalized design parameters of thermoacoustic refrigerator

Normalized parameters
$P_g/P = D$
$\theta/T_{mg} = \theta_n$
$\theta/\theta_c = \Gamma$
$c.l_2 = l_{2n}$
$c.l_3 = l_{3n}$
$c.l_4 = l_{4n}$
$c.X = X_n$
$\delta_k/y = \delta_{kn}$
$\delta_v/y = \delta_{vn}$
$Q/(PuA) = Q_n$
$W/(PuA) = W_n$

Table 2 Derived design parameters and their values as a function of the oscillating gas

Derived parameters	Helium	Air
$\lambda = u/f$	2.5 m	1.7 m
$\omega = 2\pi f$	2513.3 rads ⁻¹	1256.6 rads ⁻¹
$c = \omega/u$	2.52 m ⁻¹	3.69 m ⁻¹
$y = \delta_k$ or $2\delta_k$	@ $2\delta_k = 23.3E - 5$ m	@ $\delta_k = 5.756E - 5$ m
$l = (y - y\varepsilon)/\varepsilon$	0.411E - 4 m	0.102E - 4 m
$\sigma = \mu C_p/k_g = (\delta_v/\delta_k)^2$	0.68	0.71
$P_a = PD$	0.3 bar	0.3 bar

$$Q_{ns} = \frac{-\delta_{kn} D^2 \sin(2X_n)}{8\gamma(1+\sigma)\Lambda} \times \left[\Gamma \frac{1+\sqrt{\sigma}+\sigma}{1+\sqrt{\sigma}} - (1+\sqrt{\sigma}-\sqrt{\sigma}\delta_{kn}) \right] - \epsilon \Lambda^1 \tag{2}$$

$$W_{ns} = \frac{\delta_{kn} l_{3n} D^2}{4\gamma} \left[(\gamma-1)\epsilon \cos^2(X_n) \left(\frac{\Gamma}{(1+\sqrt{\sigma})\Lambda} - 1 \right) - \frac{\sqrt{\sigma} \sin^2(X_n)}{\epsilon \Lambda} \right] \tag{3}$$

The terms Λ^1 and Λ in Eqs.(2) and (3) are the dimensionless heat conduction correction factor and the thermal conductivity factor of the oscillating gas, respectively, are given by

$$\Lambda^1 = \frac{K_g T_{mg}}{P u l_3} \tag{4}$$

$$\Lambda = 1 - \frac{\delta_v}{y} + 0.5 \frac{\delta_v^2}{y^2} \tag{5}$$

Using the normalized equations from (2) to (5), the COP of the spiral stack is given by the ratio of the normalized cooling power output to the normalized acoustic power input is given by

$$COP_s = \frac{Q_{ns}}{W_{ns}} \tag{6}$$

Substituting the data given in Tables 1 and 2 in Eqs. (2) and (5) and the performance of the stack as a function of the normalized stack length l_{3n} and center position

X_n for helium and air are given in Tables 4 and 5. It is found that for every normalized stack length there is a maximum performance of the stack at a particular normalized stack center position for both helium and air. Hence, it is found that each stack length will have the optimum stack center position at the highest stack performance as found in the published literature [16]. But the designer chooses the optimum stack length l_3 and center position X based on ensuring the sufficient space to accommodate the loudspeaker, pressure and temperature sensors between loudspeaker and ambient heat exchanger during fabrication. Addition to these criteria the attempts are made in this section to choose the normalized stack length l_{3n} and center position X_n based on better cooling power Q at the moderate performance of the stack COP_s for both helium and air. From Tables 1 and 2 it is found that as the normalized stack length and center position increases, the performance of the stack decreases but the cooling power increases. By balancing between the stack performance and cooling power the four, stack length and center combinations (SLCC) are

Table 4 Stack performance and cooling power with helium versus the normalized stack length and normalized stack center position

l_{3n}	Helium	X_n							
		0.1	0.2	0.3	0.4	0.5	0.6	0.7	0.8
0.1	COP_s	1.80	3.29	3.75	2.88	0.82	-1.93	-4.77	-7.32
	Q (W)	190	313	334	254	75.3	-195	-546	-964
0.2	COP_s	0.99	1.86	2.39	2.54	2.33	1.85	1.21	0.513
	Q (W)	226	413	540	601	593	518	378	178
0.3	COP_s	0.68	1.28	1.68	1.86	1.83	1.64	1.35	0.99
	Q (W)	238	447	609	716	766	756	686	559
0.4	COP_s	0.52	0.97	1.29	1.45	1.47	1.37	1.19	0.96
	Q (W)	244	464	643	774	852	874	839	749
0.5	COP_s	0.42	0.78	1.04	1.19	1.22	1.16	1.03	0.87
	Q (W)	248	474	663	809	904	946	932	863
0.6	COP_s	0.35	0.66	0.88	1.00	1.04	1.00	0.90	0.78
	Q (W)	250	481	677	832	939	993	993	939
0.7	COP_s	0.3	0.56	0.76	0.87	0.90	0.87	0.80	0.70
	Q (W)	252	485	687	848	963	1030	1040	994
0.8	COP_s	0.26	0.50	0.67	0.76	0.80	0.78	0.72	0.63
	Q (W)	253	489	694	861	982	1050	1070	1030

Table 5 Stack performance and cooling power with air versus the normalized stack length and normalized stack center position

l_{3n}	Air	X_n							
		0.1	0.2	0.3	0.4	0.5	0.6	0.7	0.8
0.1	COP _s	2.53	1.96	-4.1	-13.2	-20.6	-24.8	-26.7	-27.3
	Q (W)	110	68	-132	-482	-967	-1570	-2260	-3020
0.2	COP _s	1.46	2.16	1.84	0.81	-0.42	-1.57	-2.53	-3.29
	Q (W)	152	225	211	111	-71.3	-328	-649	-1020
0.3	COP _s	1.00	1.60	1.65	1.30	0.79	0.24	-0.26	-0.70
	Q (W)	167	277	325	308	227	85.9	-111	-355
0.4	COP _s	0.77	1.25	1.37	1.21	0.92	0.59	0.26	-0.03
	Q (W)	174	303	382	407	377	293	158	-21.1
0.5	COP _s	0.62	1.02	1.15	1.07	0.88	0.65	0.41	0.20
	Q (W)	178	319	416	466	466	417	320	179
0.6	COP _s	0.52	0.87	0.99	0.94	0.81	0.63	0.45	0.28
	Q (W)	181	329	439	506	526	500	428	313
0.7	COP _s	0.45	0.75	0.87	0.84	0.73	0.60	0.45	0.31
	Q (W)	183	337	456	534	569	559	504	408
0.8	COP _s	0.39	0.66	0.77	0.75	0.67	0.56	0.44	0.32
	Q (W)	184	342	468	555	601	603	562	479

chosen (Table 6) for helium and air to study its effects on the performance of the cooler. The length of the oscillating gas (displacement amplitude) in the cold heat exchanger is given by

$$2x_1 = \frac{2P_a \sin(cx)}{\rho u \omega} \tag{7}$$

In Eq. (7), x is the location of the cold heat exchanger away from the driver (the cold end of the stack). Using the data given in Tables 1 and 2, the length of the cold heat exchanger l_4 is equal to the length of the oscillating gas ($2x_1$) is determined. It is found that the ambient heat exchanger rejects heat nearly twice the heat supplied by the cold heat exchanger [4, 5, 15]. Hence,

the length of the ambient heat exchanger l_2 is equal to $2l_4$. The normalized critical temperature gradient Γ calculated for both helium and air for the four SLCC are found to be less than one (Table 6), confirms the spiral stack behaves as refrigerator [4, 5, 13, 15–17]. The stack center position X , the position of the ambient heat exchanger l_1 , and the length of ambient heat exchanger l_2 , the length of stack l_3 , and the length of cold heat exchanger l_4 are calculated using wave number of gas, c as a function of SLCC is given in Table 6. Similar to the stack, the normalized acoustic power input to the ambient and cold heat exchangers (W_{max} and W_{ncx}) for both helium and air is calculated by setting $\Gamma=0$ (for small lengths) in Eqs. (3) and (5) as a function of

Table 6 Normalized critical temperature gradient, center position, and geometric lengths of stack-heat exchangers system as a function of the normalized stack length and center combination and working gas

He							Air						
SLCC	Γ	X (mm)	l_1 (mm)	l_2 (mm)	l_3 (mm)	l_4 (mm)	SLCC	Γ	X (mm)	l_1 (mm)	l_2 (mm)	l_3 (mm)	l_4 (mm)
$l_{3n}=0.1$	0.528	119	88	12	40	6	$l_{3n}=0.1$	0.579	54	34	7	27	3.5
$X_n=0.3$							$X_n=0.2$						
$l_{3n}=0.2$	0.361	159	103	16	80	8	$l_{3n}=0.2$	0.289	54	19	8	54	4
$X_n=0.4$							$X_n=0.2$						
$l_{3n}=0.3$	0.241	159	82	18	119	9	$l_{3n}=0.2$	0.442	81	44	11	54	5.5
$X_n=0.4$							$X_n=0.3$						
$l_{3n}=0.4$	0.233	199	98	22	159	11	$l_{3n}=0.3$	0.295	81	29	12	81	6
$X_n=0.5$							$X_n=0.3$						

SLCC is given in Table 6. The acoustic power dissipated into the stack W_s , ambient heat exchanger W_{ax} , and cold heat exchanger W_{cx} is determined by using the data given in Table 1 in the equations $W_s = W_{ns} (P\mu A)$, $W_{ax} = W_{nax} (P\mu A)$, and $W_{cx} = W_{ncx} (P\mu A)$, respectively for helium and air as a function of SLCC is given in Table 7.

3 Resonator optimization

Resonator is a solid material containing stack-heat exchangers system in the large diameter section. It should be light weight, made with poor thermal conductivity material to avoid heat leak losses and self-sufficient to withstand 10 bar in dynamic pressure. The portion of the resonator right side to the cold heat exchanger is optimized for the minimum heat dissipation losses by decreasing volume, which improves performance and power density. The quarter wavelength TDH (taper and divergent tube with hemispherical end) resonator design is efficient compared with the quarter wavelength taper and small diameter tube resonator design as found in the published literature [4, 5, 10, 18, 19]. Hence, the TDH resonator is optimized for the spiral stack with four SLCC values (Table 7) using helium and air as oscillating gas. The length of the resonator is proportional to the velocity of oscillating gas. The total length of the resonator expressed in terms of wavelength of the gas is given by

$$L_t = \frac{u}{nf} = \frac{\lambda}{n} \quad (8)$$

For full-wavelength resonator $n=1$, for half-wavelength $n=2$, for one-third-wavelength $n=3$, and for quarter wavelength $n=4$, etc. In this section the attempts are made to optimize the length, surface area and volume of the TDH resonator (Fig. 4) with helium and air as a function of the four SLCC (Table 7). For the current four SLCC resonator designs the small taper length is 20 mm, the diameter ratio at the throat is 0.15 and the radius of the hemispherical end is 100 mm, are chosen based on the minimum resonator losses [4, 5, 13, 20]. For the fixed stack diameter of 200 mm, the length of the stack diameter varies as a function of the four SLCC. The length of the divergent section L_3 decides the diverging angle θ_2 in the divergent section of the resonator and the total length of resonator L_t . The length of the divergent section is wisely chosen such that it should have small diverging angle for both helium and air (Table 8) to minimize gas turbulence during expansion. These angles are smaller compared to the published designs found elsewhere [8]. Further increase in the length of the divergent section increases the resonator length and hence the resonator

losses. This decreases the performance of the cooler and power density. The total length of the resonator L_t is expressed in terms of wavelength of gas, the total surface area of resonator (A_t), volume left to taper (VLT), volume right to taper (VRT), volume ratio (V_r , the ratio of VRT and VLT) and total volume of the resonator (V_t) is determined (Table 8). Using the data given in Tables 1 and 2 in Eq. (9), the resonator components heat power dissipation losses per unit surface area is determined [4].

$$w = 0.25u_1^2 \rho \delta_v \omega + 0.25 \frac{p_1^2 (\gamma - 1) \delta_k \omega}{\rho u^2} \quad (9)$$

The first term in the right-hand side of Eq. (9) is the viscous loss and second term is the thermal loss in the resonator system.

The pressure $p_1 = P_a \cos(cx)$ and velocity $u_1 = P_a \sin(cx) / \rho u$ in Eq. (9) are determined at the mean center position of the individual resonator component measured from the loudspeaker position. The total heat power dissipation losses for the whole resonator, W_r is determined by adding the heat power dissipation losses at the individual resonator components as given in Table 8. In the design process it is assumed that the loudspeaker provides the necessary acoustic power required for heat pumping process in the stack-heat exchangers system. The acoustic refrigeration capacity of the cooler strongly depends on the resonator power from loudspeaker. For the stack diameter of $d_1 = 200$ mm for both helium and air (Table 1), the cooling power of the stack Q is found to be 601 W for helium (Table 4) and 225 W for air (Table 5) at the optimized conditions of the normalized stack length and center combinations. Hence, the commercial loudspeaker with the power range of 500–1000 W is sufficient to power the resonator with a possibility of achieving the electroacoustic efficiency up to 90% with a back volume gas spring system (Fig. 4) [8, 21, 22]. In the real world, the designer can select the suitable commercial loudspeaker from the suppliers viz. Philips, Sony corporations, Pioneer corporation, Harman international, and many other local suppliers. The total acoustic power dissipated into the stack-heat exchangers and resonator W_r and COP, COPC, and COPR are calculated using the values given in Tables 4, 5, and 7 in Eqs. (10)–(13) as given in Table 8. For helium, at SLCC of $l_{3n} = 0.2$ and $X_n = 0.4$ the cooling power of the refrigerator is 601 W at the stack performance of 2.54 (Table 4). Further increase in the SLCC decreases the performance of the stack drastically (1.86) for the small increase of cooling power (716 W). Hence the resonator with SLCC of $l_{3n} = 0.2$ and $X_n = 0.4$ with the COP of 1.8 is optimized compared to the other three designs (Table 8) by considering the cooler performance,

Table 7 Normalized and theoretical performance results of stack-heat exchangers system as a function of the normalized stack length and center combination and working gas

He		Air													
SLCC	$Q_{rs} (10^{-5})$	$W_{rs} (10^{-5})$	$W_s (W)$	$W_{max} (10^{-6})$	$W_{sk} (W)$	$W_{rcx} (10^{-6})$	$W_{ck} (W)$	SLCC	$Q_{rs} (10^{-5})$	$W_{rs} (10^{-5})$	$W_s (W)$	$W_{max} (10^{-6})$	$W_{sk} (W)$	$W_{rcx} (10^{-6})$	$W_{ck} (W)$
$I_{3n}=0.1$	1.07	0.284	89.2	1.21	37.9	0.662	20.8	$I_{3n}=0.1$	0.636	0.325	34.8	1.48	15.9	0.887	9.5
$X_n=0.3$					54.6	1.06	33.4	$X_n=0.2$					18	1.16	12.4
$I_{3n}=0.2$	1.91	0.754	237	1.74	57.4	1.22	38.2	$I_{3n}=0.2$	2.10	0.973	104	1.68	26.4	1.87	20
$X_n=0.4$					73	1.73	54.4	$X_n=0.2$					27.6	2.31	24.7
$I_{3n}=0.3$	2.28	1.23	385	1.83	57.4	1.22	38.2	$I_{3n}=0.2$	1.97	1.07	115	2.47	26.4	1.87	20
$X_n=0.4$					73	1.73	54.4	$X_n=0.3$					27.6	2.31	24.7
$I_{3n}=0.4$	2.72	1.85	581	2.33	73	1.73	54.4	$I_{3n}=0.3$	3.04	1.84	197	2.58	27.6	2.31	24.7
$X_n=0.5$					73	1.73	54.4	$X_n=0.3$					27.6	2.31	24.7

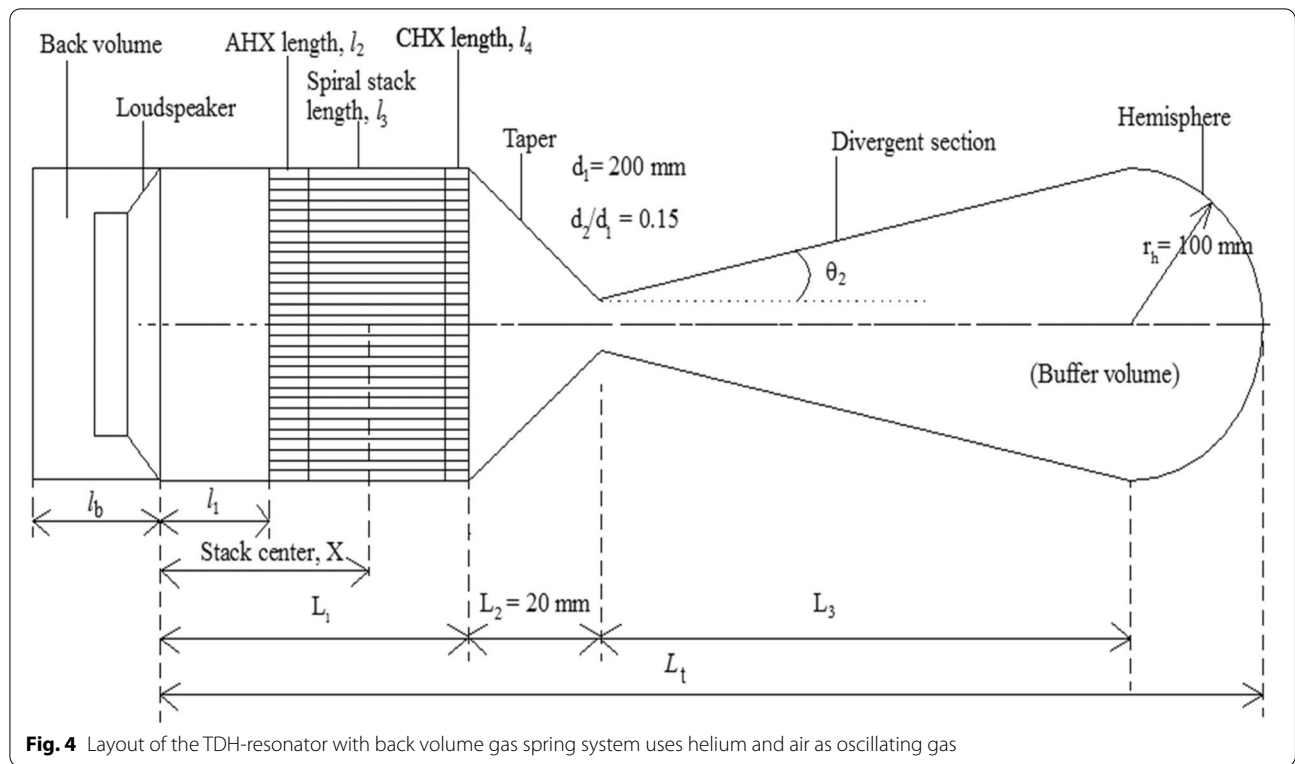


Table 8 Theoretical performance results of the optimized TDH resonator as a function of the normalized stack length and center combination and working gas

Gas	SLCC	l_3 (mm)	θ_2 (°)	L_t (mm)	A_t (m ²)	VLT (L)	VRT (L)	V_r	V_t (L)	W_r (W)	W_t (W)	COP	COPR
Helium	$l_{3n}=0.1$ $X_n=0.3$	270	17.5	535 (0.214 λ)	0.288	4.55	5.41	1.19	10.2	8.37	156	2.14	0.219
	$l_{3n}=0.2$ $X_n=0.4$	232	20.1	559 (0.224 λ)	0.314	6.49	4.95	0.76	11.7	9.21	334	1.80	0.185
	$l_{3n}=0.3$ $X_n=0.4$	223	20.9	570 (0.228 λ)	0.323	7.14	4.83	0.68	12.2	9.56	490	1.46	0.150
	$l_{3n}=0.4$ $X_n=0.5$	204	22.6	613 (0.246 λ)	0.356	9.08	4.58	0.51	13.9	10.8	719	1.19	0.122
Air	$l_{3n}=0.1$ $X_n=0.2$	193	23.7	384 (0.226 λ)	0.215	2.23	4.47	2.0	6.95	1.32	61.4	1.11	0.114
	$l_{3n}=0.2$ $X_n=0.2$	173	26.2	378 (0.222 λ)	0.217	2.68	4.21	1.57	7.14	1.11	136	1.66	0.170
	$l_{3n}=0.2$ $X_n=0.3$	150	29.4	384 (0.226 λ)	0.228	3.57	3.95	1.11	7.76	1.38	162	1.30	0.133
	$l_{3n}=0.3$ $X_n=0.3$	140	31.3	388 (0.228 λ)	0.234	4.01	3.81	0.95	8.07	1.19	250	1.30	0.133

cooling power, and the total volume of the resonator for its compact size. Similarly, the air resonator is optimized at the SLCC of $l_{3n}=0.2$ and $X_n=0.2$ with the stack performance of 2.16 at 225 W (Table 5) where the COP of the cooler is found to be 1.66 (Table 8).

$$W_t = W_s + W_{cx} + W_{ax} + W_r \tag{10}$$

$$COP = \frac{Q}{W_t} \tag{11}$$

$$\text{COPC} = \frac{T_{\text{cx}}}{\theta} \quad (12)$$

$$\text{COPR} = \frac{\text{COP}}{\text{COPC}} \quad (13)$$

4 Acoustic driver

Acoustic driver is a commercially available loudspeaker modified with back volume gas spring system. It matches the loudspeaker operating frequency with the resonator frequency, which increases the electroacoustic efficiency of the loudspeaker from 3% to 50–90% possible [4, 21, 22]. The electromechanical parameters of the commercial 1000 W loudspeaker approximately are given in Table 9.

The spring constant for the acoustic driver s is defined by

$$s = 4\pi^2 (f_d)^2 m \quad (14)$$

where f_d is the driver frequency, and m is the moving mass of the moving coil loudspeaker. Using the data given in Table 9 in Eq. (14), the spring constant for the loudspeaker with helium and air is determined. The back volume of the gas spring system for the commercial loudspeaker is given by

$$V_b = \frac{\gamma P A_b^2}{s} \quad (15)$$

where γ is the specific heats ratio, P is the average gas pressure, A_b is the cross-section of the back volume system, which is equal to the cross-section of the vibrating diaphragm of the loudspeaker, A_d . Using the data given in Tables 1 and 9, the back volume V_b and the length of the back volume l_b (Fig. 4) with helium and air resonators are found to be 3479 cm³ and 111 mm for helium, and 11,667 cm³ and 371 mm for air, respectively.

5 DeltaEC

As a check on the assumptions of the boundary layer and short stack approximations [4, 13, 23] shows that the stack length l_3 for helium and air for the chosen SLCC are smaller (Table 6) than the wavelength of the gas λ (Table 2). The temperature difference (28 K) chosen in the current research work is about a factor 10.3

smaller than the mean temperature of helium and air (288 K). The thermal and viscous penetration depths are also smaller than the half gas spacing in the stack-heat exchangers system except the thermal penetration depth of air (Tables 1 and 2). Hence the results of the calculations done in Sects. 2 and 3 are the good estimates for the design optimization of thermoacoustic cooler with helium and air. In this section, the DeltaEC computer program [12] is used to predict the performance of the theoretically optimized refrigerator models with the four SLCC operating with helium and air is discussed. DeltaEC solves the same thermoacoustic equations in a geometry designed by the user, with the boundary conditions of the different geometric component variables. The thermoacoustic segments, boundary conditions and the use of DeltaEC software for validating thermoacoustic models are discussed elsewhere [24–26]. The specifications of the loudspeaker given in Table 9 with back volume gas spring system for helium and air are used in DeltaEC calculations. In DeltaEC program, the cold and ambient heat exchangers are targeted at 273 K and 301 K, respectively and hence the mean temperature of the heat exchangers T_{mx} is 287 K. The cooler is operated with 10 bar helium and air with 3% drive ratio. In the theoretical design calculations, the mean temperature of gas T_{mg} is taken to be 288 K, 1 K higher than the mean temperature of the heat exchangers 287 K as found in the published literature [4, 7, 8]. Similarly, the DeltaEC predicts the mean temperature of gas T_{mg} is about 0.28 to 0.74 K higher than the mean temperature of the heat exchangers T_{mx} with helium and air as given in Table 10. It increases slightly as the SLCC increases. DeltaEC assumes perfect insulation for the whole resonator including the loudspeaker with back volume gas spring system [13, 26]. Hence, the AHX rejects the heat equal to the sum of heat absorbed at CHX and the electrical energy input to the loudspeaker with helium and air for the four SLCC as given in Table 10. The electrical power input to the driver W_e and the heat rejection rate at the AHX Q_r increases with increase in the SLCC for both helium and air. This is because of the increase in volume of the stack demands higher electrical power input for heat pumping and hence the heat rejection rate at the AHX increases. The electro-acoustic efficiency of the loudspeaker with back volume gas spring system increases with increase in the SLCC (29.5–87.9%) for both helium and air (Table 10). This is because of the decrease in acoustic resistance due

Table 9 Electromechanical parameters of the loudspeaker with gas spring system for helium and air as working substance

A_d (@ $d_1 = 20$ cm) = 314.2 cm ² , $R_e = 12 \Omega$, $L_e = 0.0039$ H, $Bl = 75$ T-m, $m = 75$ g, $s = 473.7$ kNm ⁻¹ (helium @ $f_d = 400$ Hz), $s = 118$ kNm ⁻¹ (air @ $f_d = 200$ Hz), $R_m = 9$ Nsm ⁻¹
--

Table 10 DeltaEC results of the optimized TDH resonator design as a function of the normalized stack length and center combination and working gas (Helium at 400 Hz and air at 200 Hz)

Gas	SLCC	T_{mg} (K)	Q_r (W)	W_e (W)	η_{ea} (%)	Q (W)	COP	COPR
Helium	$l_{3n}=0.1$ $X_n=0.3$	287.31	497.9	281.5	58.9	216.4	1.306	0.134
	$l_{3n}=0.2$ $X_n=0.4$	287.44	796.7	447.3	78.3	349.4	0.998	0.102
	$l_{3n}=0.3$ $X_n=0.4$	287.70	950.3	593.9	84.5	356.4	0.710	0.073
	$l_{3n}=0.4$ $X_n=0.5$	287.74	1157	834.6	87.9	322.4	0.439	0.045
Air	$l_{3n}=0.1$ $X_n=0.2$	287.28	266.7	194.4	29.5	72.3	1.260	0.129
	$l_{3n}=0.2$ $X_n=0.2$	287.64	392.6	253.9	48.2	138.7	1.133	0.116
	$l_{3n}=0.2$ $X_n=0.3$	287.34	441.7	297.0	56.9	144.7	0.856	0.088
	$l_{3n}=0.3$ $X_n=0.3$	287.57	550.2	381.6	68.1	168.6	0.649	0.067

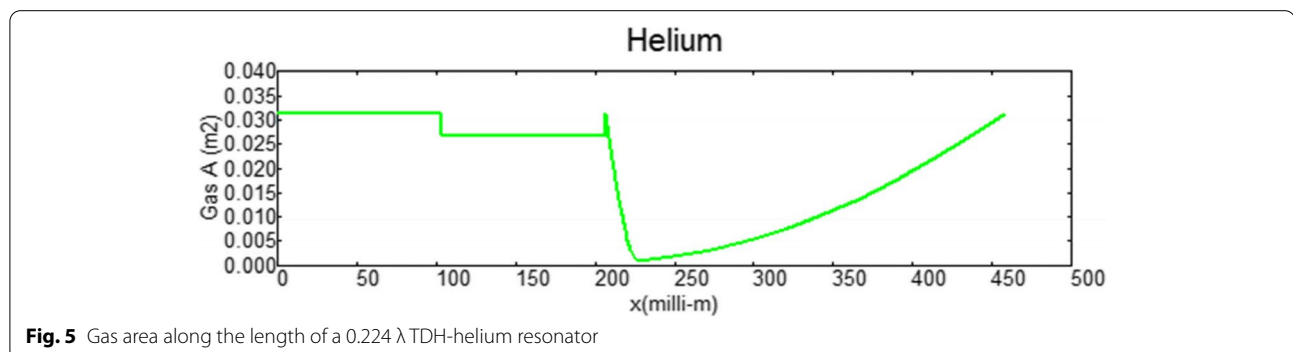
to gas turbulence in the stack-heat exchangers system. DeltaEC predicts that the cooling power of the refrigerator increases with increase in the SLCC, whereas the COP and COPR decreases (Table 10) similar to the theoretical results (Table 8). For the optimized 0.224λ TDH-helium, and the 0.222λ TDH-air resonators (Table 8), the variation of the gas area Gas A, acoustic peak pressure amplitude P_a , and solid material temperature T_s , along the resonator length from the driver position are shown in Figs. 5, 6, 7, 8, 9, and 10.

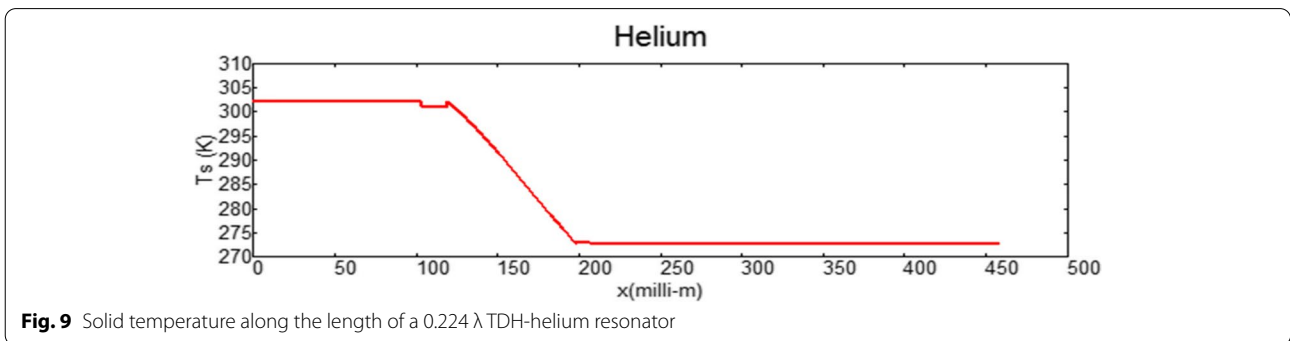
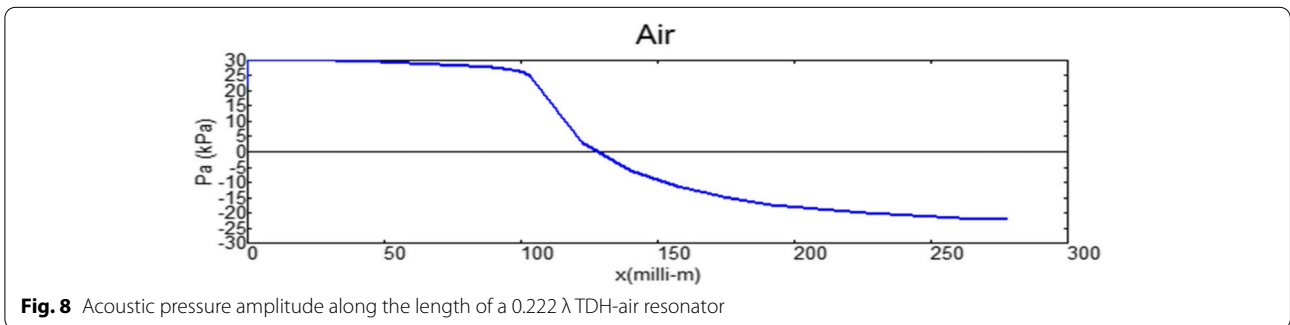
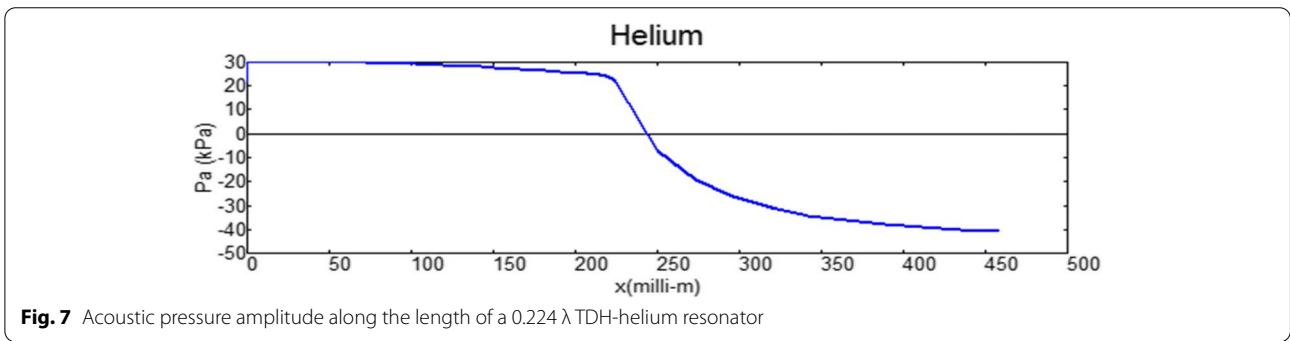
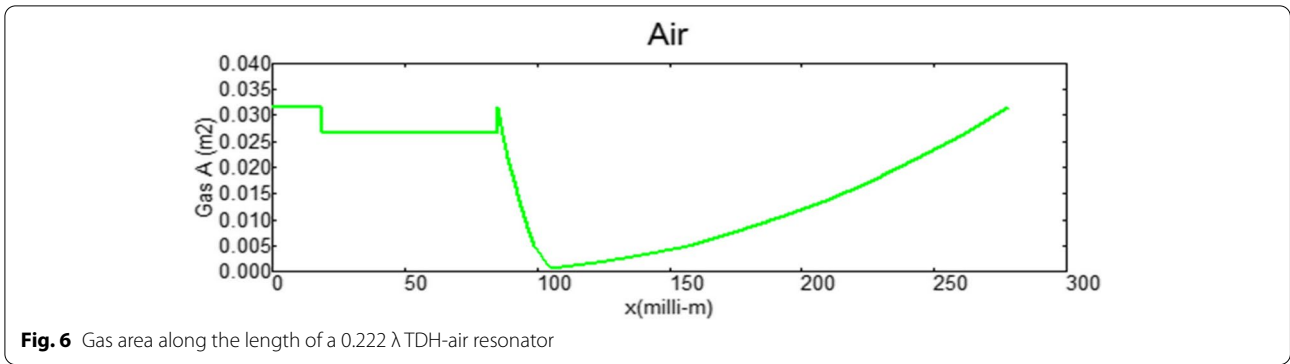
The gas area between the driver and AHX is 100% which is equal to the cross-section area of the stack 0.03142 m^2 . There is a 15% reduction in gas area in the stack-heat exchangers system, which drastically decreases in the taper section, and gradually increase in the divergent section terminated with the hemispherical end. DeltaEC shows the same nature of variation of gas area in the resonator for both helium and air as shown in Figs. 5 and 6. The only difference is the position and the length of the stack-heat exchangers system. The acoustic pressure amplitude

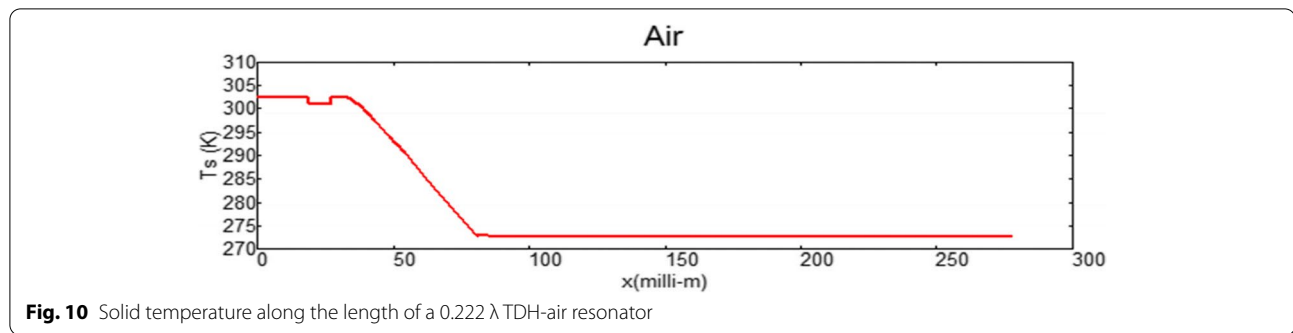
of gas at the driver position is 0.3 bar, remains same up to the length of AHX position, and gradually decrease in the stack-heat exchangers system. Also decreases drastically in the taper section and further goes negative in the divergent section for both helium and air as observed in Figs. 7 and 8. The variation of solid material temperature T_s (stack-heat exchangers and resonator) from the driver position to the resonator tip for helium and air is shown in Figs. 9 and 10. There is a small drop of temperature of about 2 K in AHX, and decrease drastically in the stack region, reaches to 273 K in the CHX region. The temperature of the resonator remains the same for the rest of the portion for both helium and air since the DeltaEC assumes perfect insulation.

6 Conclusions

The design and optimization of the thermoacoustic refrigerators having 200 mm diameter spiral stack-heat exchangers system with 85% porosity operating with helium and air at 10 bar pressure and 3% drive ratio for

**Fig. 5** Gas area along the length of a 0.224λ TDH-helium resonator





the temperature difference of $28 \text{ }^\circ\text{C}$ is discussed. In the design process, the AHX is assumed to be kept at $28 \text{ }^\circ\text{C}$ by water cooling system. The stack-heat exchangers system is optimized by considering both performance of the stack and cooling power. This improves performance as well as power density of the refrigerator as discussed in Sects. 1, 2, and 3. The current optimized 0.224λ TDH-helium resonator has 2% improvement in COP, 79% improvement in cooling power and 3.1 times increase in power density compared to the published design [8]. But the optimized 0.222λ TDH-air resonator has 83% improvement in COP leading to 27% decrease in cooling power and 2.2 times increase in power density compared to the published design [8]. It is found that the air shows little poor performance compared to helium because of its low sound velocity and thermal conductivity (Table 1) and high Prandtl number (Table 2). But the cost of air is much cheaper and abundantly available in nature compared to helium, and hence the use of air as working gas is justifiable. The theoretical and DeltaEC results (Tables 8 and 10) show agreement with each other but the theoretical results show better performance compared to DeltaEC results. Because the theoretical design is optimized by neglecting loudspeaker parameters, and neglecting the effect of damping in the right portion of the resonator after CHX (Fig. 4). This affects the velocity of oscillating gas and frequency and hence the performance of the cooler [4, 5]. Similar to helium and air, the design and optimization techniques discussed in this paper to improve performance, cooling power and power density of the thermoacoustic coolers are also holds good for the other working substances used elsewhere [4, 12, 27].

7 Nomenclature

A Cross-sectional area of stack, m^2
 AHX Ambient heat exchanger
 A_b Cross-sectional area of the back volume system
 A_d Cross-sectional area of vibrating diaphragm of loudspeaker, cm^2

A_t Total resonator surface area, cm^2
 B_l Force factor, NA^{-1} or T-m
 CHX Cold heat exchanger
 COP Coefficient of performance of cooler
 COPC Carnot's Coefficient of performance
 COPR Coefficient of performance relative to Carnot's
 COP_s Coefficient of performance of stack
 c Wave number of gas, cym.^{-1}
 C_p Specific heat of gas at constant pressure, $\text{Jkg}^{-1} \text{K}^{-1}$
 C_v Specific heat of gas at constant volume, $\text{Jkg}^{-1} \text{K}^{-1}$
 D Drive ratio
 DeltaEC Design environment for low-amplitude thermoacoustic Energy Conversion
 d_1 Stack diameter, mm
 d_2 Throat diameter, mm
 f Resonator frequency, Hz
 f_d Driver frequency, Hz
 Gas A Gas area in resonator system, m^2
 k_g Thermal conductivity of gas, $\text{Wm}^{-1}\text{K}^{-1}$
 LDTAR Loudspeaker-driven thermoacoustic refrigerator
 L_1 Length of large diameter tube, m
 L_2 Length of taper tube, m
 L_3 Length of divergent tube, m
 L_e Electrical inductance of loudspeaker, H
 L_t Total resonator length, mm
 l Half spiral stack sheet thickness, mm
 l_1 Distance between loudspeaker and hot heat exchanger, mm
 l_2 Length of ambient heat exchanger, mm
 l_3 Length of stack, mm
 l_4 Length of cold heat exchanger, mm
 l_b Length of back volume system, mm
 m Moving mass of driver, g
 P Average gas pressure, bar
 PVC Poly vinyl chloride
 Pv Pressure and volume
 Ph Pressure and enthalpy
 P_a Acoustic or dynamic pressure amplitude, bar
 p_1 Pressure of gas at the mean center position of the component, bar

P_c Power density of cooler, Wm^{-3}
 Q Cooling power, W
 Q_r Heat rejected by ambient heat exchanger, W
 R_m Mechanical resistance of loudspeaker, Nsm^{-1}
 R_e Electrical resistance of loudspeaker, Ω
 r_h Hemispherical radius, mm
 s Loudspeaker spring stiffness, Nm^{-1}
 SLCC Stack length and center combination
 EDTAR Engine-driven thermoacoustic refrigerator
 TDH Taper and divergent tube with hemispherical end
 T_s Temperature and entropy
 T_{cx} Temperature of cold heat exchanger, K
 T_{ax} Temperature of ambient heat exchanger, K
 T_{mg} Mean temperature of gas between heat exchangers, K
 T_{mx} Mean temperature of ambient and cold heat exchangers, K
 T_s Solid material temperature, K
 u Velocity of oscillating gas, ms^{-1}
 u_1 Velocity of gas at the mean center position of the component, ms^{-1}
 VLT Volume left to taper, L
 VT Volume of taper, L
 VRT Volume right to taper, L
 V_r Resonator volume ratio
 V_t Total resonator volume, L
 W Acoustic power, W
 W_e Electrical power input to loudspeaker, W
 W_r Acoustic power dissipation in resonator, W
 W_s Acoustic power dissipation in stack, W
 W_{ax} Acoustic power dissipation in ambient heat exchanger, W
 W_{cx} Acoustic power dissipation in cold heat exchanger, W
 W_t Total acoustic power dissipated in stack, heat exchangers and resonator, W
 w Acoustic power loss per unit surface area of resonator, Wm^{-2}
 X Stack center position, mm
 x Component position away from the driver, m
 y Half gas spacing in stack-heat exchangers sheet, mm
 Greek symbols
 δ_k Thermal penetration depth, mm
 δ_v Viscous penetration depth, mm
 ε Porosity of stack-heat exchangers system.
 β Thermal expansion coefficient, K^{-1}
 γ Ratio of specific heats
 Γ Normalized critical temperature gradient.
 ρ Mass density of gas, kgm^{-3}
 η_{ea} Electro-acoustic efficiency of the loudspeaker, %
 σ Gas Prandtl number
 λ Wavelength, m
 ω Angular frequency of acoustic wave, rads^{-1}
 μ Dynamic viscosity of working gas, $\text{kgm}^{-1}\text{s}^{-1}$

θ Temperature difference between hot and cold heat exchangers, K
 θ_c Critical temperature difference between hot and cold heat exchangers, K
 θ_n Normalized temperature gradient between hot and cold heat exchangers
 θ_2 Diverging angle in the buffer volume, degree

Subscripts

c Critical
 n Normalized, number.
 s Stack
 t Total

Acknowledgements

This work was supported by JSSMVP Mysuru, Principal, HOD (Mechanical), and all the staff of the Department of Mechanical Engineering, JSSATE Bengaluru. Authors thank Bill Ward, John Clark, and Greg Swift, Los Alamos National Laboratory, USA, for developing DeltaEC software and making it freely available for research purpose.

Authors' contributions

The author(s) read and approved the final manuscript.

Availability of data and materials

All data generated or analyzed during this study are included in this article.

Declarations

Competing interests

The authors declare that they have no competing interests.

Author details

¹Department of Mechanical Engineering, JSS Academy of Technical Education, Dr. Vishnuvardhana Road, Bengaluru 560 060, India. ²Department of Mechanical Engineering, Indian Institute of Science, Bengaluru 560 012, India. ³Formerly Central Power Research Institute, Bengaluru 560 080, India. ⁴Department of Mechanical Engineering, Dayananda Sagar University, Hosur Road, Bengaluru 560 068, India.

Received: 17 March 2022 Accepted: 28 June 2022

Published online: 28 July 2022

References

- Babaei, H., & Siddiqui, K. (2008). Design and optimization of thermoacoustic devices. *Energy Conversion and Mgmt.*, 49, 3585–3598.
- Prashantha, B. G., Govinde Gowda, M. S., Seetharamu, S., & Narasimham, G. S. V. L. (2013). Theoretical evaluation of loudspeaker for a 10-W cooling power thermoacoustic refrigerator. *International Journal Air-Conditioning and Refrigeration.*, 21(4), 1350027. <https://doi.org/10.1142/S2010132513500272> (8 pages).
- Prashantha, B. G., Govinde Gowda, M. S., Seetharamu, S., & Narasimham, G. S. V. L. (2013). Design and analysis of thermoacoustic refrigerator. *International Journal Air-Conditioning and Refrigeration.*, 21(1), 1350001. <https://doi.org/10.1142/S2010132513500016> (10 pages).
- Tijani M.E.H. (2001) *Loudspeaker-driven thermo-acoustic refrigeration*. Ph.D. Thesis, Eindhoven University of Technology
- Prashantha, B. G., Govinde Gowda, M. S., Seetharamu, S., & Narasimham, G. S. V. L. (2017). Design construction and performance of 10 W thermoacoustic refrigerators. *International Journal Air-Conditioning and Refrigeration.*, 25(3), 1750023. <https://doi.org/10.1142/S2010132517500237> (14 pages).
- Prashantha, B. G., Seetharamu, S., Narasimham, G. S. V. L., & Praveen Kumar, M. R. (2019). Effect of stack spacing on the performance of thermoacoustic refrigerators Using Helium and Air as Working Substances.

- International Journal Air-Conditioning and Refrigeration.*, 27(2), 1750023. <https://doi.org/10.1142/S2010132519500160> (11 pages).
7. Prashantha, B. G., Swamy, D. R., Bhimasen Soargaon, & Nanjundeswaraswamy, T. S. (2020). Design optimization and analysis of thermoacoustic refrigerators. *International Journal Air-Conditioning and Refrigeration.*, 28(3), 2050020. <https://doi.org/10.1142/S2010132520500200> (12 pages).
 8. Prashantha, B. G., Narasimham, G. S. V. L., Seetharamu, S., & Manjunatha, K. (2021). Effect of gas blockage on the theoretical performance of thermoacoustic refrigerators. *International Journal Air-Conditioning and Refrigeration.*, 29(3), 2150026. <https://doi.org/10.1142/S2010132521500267> (16 pages).
 9. Prashantha, B. G., Govinde Gowda, M. S., Seetharamu, S., & Narasimham, G. S. V. L. (2014). Design and optimization of a loudspeaker-driven 10 W cooling power thermoacoustic refrigerator. *International Journal Air-Conditioning and Refrigeration.*, 22(3), 1450015. <https://doi.org/10.1142/S2010132514500151> (15 pages).
 10. Prashantha, B. G., Govinde Gowda, M. S., Seetharamu, S., & Narasimham, G. S. V. L. (2017). Design and comparative analysis of thermoacoustic refrigerators. *International Journal Air-Conditioning and Refrigeration.*, 25(1), 1750002. <https://doi.org/10.1142/S201013251750002X>
 11. Petculescu G. (2002). *Fundamental measurements in standing-wave and travelling-wave thermoacoustics*. Ph.D. thesis, OHIO University
 12. Ward B. Clark J. & Swift G.W. (2008). Design environment for low-amplitude thermoacoustic energy conversion (DeltaEC software). Version 6.2, Los Alamos National Laboratory. Available at <http://www.lanl.gov/thermoacoustics>.
 13. Prashantha B. G., Govinde Gowda M. S., Seetharamu S. & Narasimham G. S. V. L. (2018). Design and analysis of acoustically-driven 50 W thermoacoustic refrigerators. *Sādhanā*. 43 (82), (13 pages). <https://doi.org/10.1007/s12046-018-0860-8>
 14. Olson, J. R., & Swift, G. W. (1994). Similitude in thermoacoustic. *Journal of the Acoustical Society of America*, 95(3), 1405–1412.
 15. Swift, G. W. (1988). Thermoacoustic engines. *Journal of the Acoustical Society of America*, 84(4), 1145–1180.
 16. Kim, Y.T., & Kim, M. G. (2000). Optimum positions of a stack in a thermoacoustic heat pump. *Journal of the Korean Physical Society*, 36(5), 279–286.
 17. Rott, N. (1980). Thermoacoustics. *Advances in Applied Mechanics*, 20, 135–175.
 18. Prashantha, B. G., Govinde Gowda, M. S., Seetharamu, S., & Narasimham, G. S. V. L. (2016). Design analysis of thermoacoustic refrigerator using air and helium as working substances. *International Journal of Thermal and Environmental Engineering.*, 13(2), 113–120. <https://doi.org/10.5383/ijtee.13.02.006>
 19. T.J. Hofler, Thermoacoustic refrigerator design and Performance, Ph.D. thesis, University of California, San Diego (1986).
 20. Garrett, S. L., Adef, J. A., & Hofler, T. J. (1993). Thermoacoustic refrigerator for space applications. *Journal of Thermophysics and Heat Transfer*, 7, 595–599.
 21. Wetzal, M., & Herman, C. (1997). Design optimization of thermoacoustic refrigerator. *International Journal of Refrigeration*, 20(1), 3–21.
 22. Prashantha, B. G., Govinde Gowda, M. S., Seetharamu, S., & Narasimham, G. S. V. L. (2013). Theoretical evaluation of 10-W cooling power thermoacoustic refrigerator. *Heat Transfer-Asian Research Journal*, 43(7), 557–591. <https://doi.org/10.1002/htj.21094>
 23. Zolpakar N.A., Mohd-Ghazali N., and El-Fawal M.H., Performance analysis of the standing wave thermoacoustic refrigerator: a review, renewable and sustainable energy reviews, 54 (2016) 626–634.
 24. Prashantha, B. G., Govinde Gowda, M. S., Seetharamu, S., & Narasimham, G. S. V. L. (2015). Resonator optimization and studying the effect of drive ratio on the theoretical performance of a 10-W cooling power thermoacoustic refrigerator. *International Journal of Air-Conditioning and Refrigeration.*, 23(3), 1550020. <https://doi.org/10.1142/S2010132515500200> (12 pages).
 25. Prashantha, B. G., Seetharamu, S., Narasimham, G. S. V. L., & Praveen Kumar, M. R. (2019). Design and analysis of thermoacoustic refrigerators using air as working substance. *International Journal of Air-Conditioning and Refrigeration.*, 27(1), 1950008. <https://doi.org/10.1142/S2010132519500081> (14 pages).
 26. Swift, G. W. (2002). Thermoacoustics: A unifying perspective of some engines and refrigerators. *Acoustical Society of America.*, 113, 214–218.
 27. Prashantha, B. G., Govinde Gowda, M. S., & Seetharamu, S. (2013). Effect of mean operating pressure on the performance of stack-based thermoacoustic refrigerator. *International Journal Thermal and Environmental Engineering.*, 5(1), 83–89. <https://doi.org/10.5383/ijtee.05.01.009>